Available online at www.sciencedirect.com
SCIENCE DIRECT®
ELSEVIER
Applied Surface Science 217 (2003) 202–209
applied surface science
www.elsevier.com/locate/apsusc

Laser ablation of CsI analyzed by delayed extraction

F. Fernández-Lima[a], V.M. Collado[b], C.R. Ponciano[b], L.S. Farenzena[b], E. Pedrero[c], E.F. da Silveira[b,*]

[a]*Instituto Superior de Ciencias y Tecnologías Nucleares, Ave Salvador Allende esq. Luaces, s/n CP 10600, AP. 6163, Ciudad de la Habana, Cuba*
[b]*Pontifícia Universidade Católica, CP 38071, Rua Marques de Sao Vicente 225, G. Physics, Rio de Janeiro 22452-970, Brazil*
[c]*Physics Faculty-IMRE, University of Havana, Havana, Cuba*

Received 21 August 2002; received in revised form 21 August 2002; accepted 22 March 2003

Abstract

Secondary ion emission from polycrystalline CsI irradiated by pulsed-UV laser (337 nm) is analyzed by time-of-flight (TOF) mass spectrometry. Measurements were performed for different laser intensities and for several delayed extraction times (0–200 ns). The TOF peak shape is characterized by a Gaussian-like structure (fast component), followed by a tail (slow component) that is more pronounced when the extraction field is delayed. A thermal-sputtering uni-dimensional model is employed to describe the solid surface and plasma temperatures as a function of time. Heat diffusion, vapor photo-ionization, radiative emission and plume expansion are considered. Within the approximations used, the model predicts reasonable drift velocities of the plume ($\approx$1.4 km s^{-1}) but very high plasma temperatures ($\approx 10^5$ K). The width of the TOF peak fast component allows determination of the plume temperature during its expansion.

PACS: 81.15.Fg; 82.80.Ms; 52.50.Jm; 52.50.-m

Keywords: Laser ablation; Plasma diagnostic; Plasma temperature; TOF; Delayed extraction

1. Introduction

Pulsed laser ablation is a common method to grow thin films of a wide range of materials, such as metals, superconductors, semiconductors and insulators. The chemical activity and stickiness of deposited films are properties that depend on energy distributions of the laser ablated species. Therefore, it is important to investigate how to control these distributions to produce high quality films. A great effort has been devoted to the understanding of this subject [1].

Laser-generated plasmas have special characteristics which are attributed to the high evaporation flux rates and to the interaction of the laser radiation with the evaporated material; in particular, pulsed-laser evaporation has been found to be significantly different from other vaporization methods. This high evaporation rate is obtained by heating the solid above the normal boiling point with powerful laser pulses, producing an ionized plume formed by ions that move with kinetic energies up to 100 eV [2,3]. The vapor evolved from the hot solid surface absorbs strongly the

* Corresponding author. Tel.: +55-21-31141272; fax: +55-21-31141275.
E-mail address: enio@fis.puc-rio.br (E.F. da Silveira).

0169-4332/03/$ – see front matter © 2003 Elsevier Science B.V. All rights reserved.
doi:10.1016/S0169-4332(03)00547-6

laser radiation through three major processes: inverse bremsstrahlung (IB), multiphoton ionization (MPI) and thermal runaway [4]. In many cases, IB is not sufficient to sustain plasma formation, and particularly for ultraviolet (UV) lasers, the need to include photo-ionization has been pointed out [5,6].

Several approaches have been made to describe the laser ablation process: analytical models, based on self-regulating absorption via IB [7], work well when the laser intensity is high enough to fully-ionize the plasma in the early stage of the pulse; models considering that the vapor absorption reduces the amount of material removed [3] (without heating or producing ionization in the vapor); models assuming that photo-absorption (photo-ionization of the excited states) and collisional processes produce plasma [5]; model including the shielding of the target by IB [8]; and numerical models based on solid heating and evaporation by laser, as well as vapor heating, ionization and expansion [9].

Cesium iodide and other alkali halides are very good electron-emitting materials, being also used for γ- and X-rays radiation conversion into UV. This makes CsI a widely studied material for application in charged particle scintillator and photo-detectors, such as the Ring-Imaging Cherenkov (RICH) detectors [10–12]. It is therefore important to understand how ionizing radiation interacts, damages and ablates CsI. In addition, this material has a relatively simple chemical composition, both atomic species being mono-isotopic, which simplifies mass-spectrometric analyses.

In this article, experimental results and model predictions of laser sputtering of cesium iodide are presented. A linear time-of-flight mass spectrometer equipped with delayed extraction field ion source was used for the Cs ion sputtering analysis. A thermal model [9] is employed to describe the heating and vaporization, by the laser, of the target and the plume. Laser absorption leading to heating and ionization of the vapor is considered together with re-radiation to the condensed phase at the target surface.

2. Theory

The laser ablation of solids involves a number of complex interacting physical processes in the solid and inside the vapor phase of the emitted material. In the condensed phase there is a need to consider the reflection and absorption of the laser beam by the target, as well as the thermal conduction through the solid and the evaporation dynamics. The physical properties associated with these processes are temperature dependent. The next step is to consider the absorption and the reflection of the laser radiation by the formed vapor, once these two processes reduce the laser intensity (energy flux) that reaches the target. The heated and ionized vapor generates a high pressure that drives its rapid expansion away from the target surface, tending to lower its density and temperature.

In this work, the numerical treatment of generation, thermal evolution and expansion of the plume has been performed in three stages: (i) solid heating, (ii) laser-plume interaction and (iii) Cs^+ ion motion inside the spectrometer. A complete description of the first two processes is very difficult and approximations are made. In particular, to simplify the plume expansion description, it is assumed in the model that the plume temperature does not depend on position and that the plume velocity (v_{drift}) becomes constant when the laser pulse vanishes. Moreover, only the fast component of the TOF peak is considered for analysis. The slow component (peak tail) is probably formed by a small fraction of flying ions undergoing more collisions than those of the fast component and requires a more precise theoretical treatment.

2.1. First stage: solid heating before sublimation

The laser spot, about 50 μm of diameter in our measurements, turns out to be much larger than 0.25 μm, the measured penetration depth (k_a^{-1}) of a 337 nm laser radiation inside the polycrystalline CsI target. Such depth value is comparable to $k_a^{-1} = 0.12$ μm which has been reported for UV absorption by CsI crystals [13]. This large diameter/depth ratio allows the use of the uni-dimensional diffusion equation to describe the solid temperature as a function of time and depth [14]:

$$\rho C \frac{\partial T}{\partial t} = \frac{\partial}{\partial x}\left(K \frac{\partial T}{\partial t}\right) + (1 - R_{lt}) I k_a \, e^{-k_a x} \tag{1}$$

where ρ, C, K, k_a, I and R_{lt} are the mass density, specific heat, thermal conductivity, absorption coefficient,

energy flux and reflectivity of the material, respectively. Considering that these parameters are neither temperature nor position dependent, this equation can be solved analytically [15]. The values, adequate for CsI, $\rho = 4.51\ \mathrm{g\ cm^{-3}}$, $C = 0.173\ \mathrm{J\ g^{-1}\ K^{-1}}$, $K = 1.05 \times 10^2\ \mathrm{W\ cm^{-1}\ K^{-1}}$, $k_a^{-1} = 0.25\ \mu\mathrm{m}$, $I = 7.6 \times 10^8\ \mathrm{W\ cm^{-2}}$ and $R_{lt} = 0.04$ [16] were used in the calculation. It has been found that the surface temperature T_s rises almost linearly from the initial target temperature, $T_0 = 300$ K, to the boiling temperature, $T_b = 774$ K (of CsI at 10^{-6} mbar pressure), in a time interval of 4.5×10^{-3} ns. This value is almost three orders of magnitude shorter than the laser pulse width (3 ns in our case). Moreover, in this time range, the temperature inside the crystal decreases exponentially as function of the depth x, revealing that heat diffusion process is much slower than the energy deposition one at the end of the laser pulse T_s would increases up to 10^5 K if no phase transformation occurs, showing that material emission is unavoidable.

2.2. Second stage: sublimation, vapor ionization and heating

Sublimation of alkali halides differs from that of covalent or molecular materials in the sense that emitted ions are preformed and may recombine very fast. However, in order to apply the usual assumption of ablation models about the neutral nature of emitted species, it is assumed that the CsI plasma is promptly neutralized.

Two processes of plasma heating are considered, the inverse-bremsstrahlung (IB) and the multiphoton ionization (MPI). We have evaluated the IB heating through the procedure employed by [6,17]; a negligible temperature increase was found. On the other hand, the MPI process, even in its single-photon mode, reveals to be very efficient.

In this case, and with the purpose of describing laser absorption in a relatively simple laser ablation model, a typical absorption cross-section to both atoms and ions was assigned. The value is assumed to be the threshold value of the hydrogen-like photo-ionization cross section as given in [18]:

$$\sigma_p(\mathrm{cm^2}) = 7.9 \times 10^{-18} \left(\frac{E_I^*}{h\nu}\right)^3 \left(\frac{I_H}{E_I^*}\right)^{1/2} \tag{2}$$

where I_H is the ionization potential of hydrogen and E_I^* the typical ionization energy of the excited states which can be photo-ionized. In the current calculations, E_I^* is taken to be equal to the laser photon energy $h\nu = 3.68$ eV ($\lambda = 337$ nm for nitrogen laser), resulting in $\sigma_p = 1.5 \times 10^{-17}\ \mathrm{cm^2}$.

As a consequence of the analysis using Eq. (1), the heat diffusion to the bulk during the laser pulse is considered negligible. Therefore, the target surface temperature, after the melting and vaporization processes had started, is given by [2]:

$$T_s(t) = T_0 - \frac{L_f}{C} + \frac{k_a}{\rho C} \int_0^t I_s(\tau)\, \mathrm{d}\tau \tag{3}$$

where I_s is the energy flux converted into heat at the surface and L_f the heat of fusion. If N is the average plasma density and l is the thickness of the layer, I_s is the balance of three contributions: laser irradiation (attenuated by the plasma), plasma irradiation and vaporization cooling:

$$I_s = (1 - R_{lp})(1 - R_{lt}) I_l \exp\left(\frac{-\sigma_p N l}{\cos\theta}\right) + (1 - R_{pt}) I_p - \frac{\mathrm{d}(Nl)}{\mathrm{d}t} L_v \tag{4}$$

where I_l is the input laser irradiance, θ the incidence angle of the laser, $I_p = \sigma T^4 (1 - \exp(-\sigma_p N l))$ the irradiance emitted by the plasma [19], σ the Stefan–Boltzmann constant, R_{lp} the plasma reflectivity for the laser irradiation, R_{pt} the target reflectivity for plasma irradiation and L_v is the heat of vaporization per atom.

The flux of particles undergoing phase transformation is

$$\frac{\mathrm{d}(Nl)}{\mathrm{d}t} = P_v(T_b) \exp\left[\frac{L_v}{k_b}\left(\frac{1}{T_b} - \frac{1}{T_s}\right)\right] \sqrt{\frac{m}{2\pi k_b T_s}} \tag{5}$$

where k_b is the Boltzmann constant and m the mass of the ejected particles. The vapor pressure P_v (T_b) is controlled by the Clausiuss–Clapeyron equation [20,21].

Vaporized material is added to the plasma at a temperature equal to T_s. The plasma temperature T_p is found by considering the power absorbed from the laser and the power loss by self-emission from the plasma. Thus, the rate of the plasma temperature

variation is given by [10]:

$$\frac{d(k_b T_p)}{dt} Nl\gamma(Z+1)\left[\frac{{M_a}^2}{2}+\frac{1}{\gamma(\gamma-1)}\right] = I_l\left[1+R_{lt}(1-R_{lp})\exp\left(\frac{-\sigma_p Nl}{\cos\theta}\right)\right] \times\left[1-(1-R_{lp})\exp\left(\frac{-\sigma_p Nl}{\cos\theta}\right)\right]-(2-R_{lp})I_p \quad (6)$$

M_a is the Mach number of the plasma flow, and following Phipps [11], is taken to be 1. The specific heat ratio γ is taken to be 1.33. Since the plasma is considered to be expanding at the sound velocity, the thickness of the plasma layer increases with the velocity:

$$\frac{dl}{dt}=\sqrt{\frac{\gamma(Z+1)k_b T_p}{m}} \quad (7)$$

Eqs. (3)–(6), which describe the evolution of the surface temperature and of the vaporized material during the laser pulse, were numerically integrated using MathCAD. In the calculation, the values of $R_{lp}=0.25$ and $L_f=90.8\ \mathrm{J\ g^{-1}}$ [14] were used.

2.3. Third stage: ion dynamics in the TOF spectrometer

The third stage initiates when no more energy is brought into the plasma by the laser. Then, the plume starts to cool down by three processes: radiation emission, heat transfer to solid and expansion into vacuum. At the beginning, the plume accelerates axially, due to interaction with the solid, up to stabilize in a constant drift velocity. When the extraction field is applied, the ions of the plume are accelerated again. The plasma temperature at this moment can be estimated by the fitting of the experimental TOF peak shape of the detected ions. The input parameters for the ion TOF calculation are the plasma drift velocity (v_{drift}) and its center of mass position calculated according the second stage description. The drift velocity is determined from the plasma temperature when the laser pulse vanishes, assuming that no more target material is substantially extracted after this moment. In addition, as a constant plasma density is also assumed, the position of the plasma center of mass is determined by using the Eq. (7). A shift-Gaussian-like axial velocity distribution $P(v)$ is considered in the TOF peak calculation:

$$P(v)=P_0\exp\left(-\frac{m(v-v_{drift})^2}{2k_b T_{fast}}\right) \quad (8)$$

where T_{fast} is the free parameter that essentially controls the TOF peak width. This quantity represents the plasma temperature of an expanding system, which center of mass moves with a velocity v_{drift}.

3. Experimental

The experiments were performed in a two-acceleration region linear mass spectrometer equipped with a delayed field extraction (DE) system. The 337 nm radiation from a nitrogen laser (Laser Science, Inc.) is brought into focus on the target with a 30° incidence angle.

The ions are detected with a microchannel plate system and the delivered signals are sampled at a rate of 500 MHz by a Tektronix TDS 520B digital oscilloscope (2 ns resolution). CsI polycrystalline films were grown by deposition in an evaporation chamber at a pressure of 10^{-5} mbar.

The ion extraction region is composed of two stages (Fig. 1), each one ending by a 90% transmission grid. Leakage field effects, due to the acceleration grid structure, were taken into account [22]. The distance d_1 from the target to the first grid is 4.5 ± 0.1 mm; the distance d_2 from the first to the second grid is 20.0 ± 0.1 mm. The drift tube length L is 276.5 ± 0.1 mm. The delayed extraction was set in such way

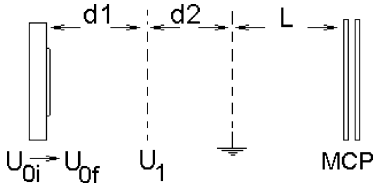

Fig. 1. Two-acceleration region linear mass spectrometer, prepared for ion delayed extraction. After the laser shot, the formed plume expands in an essentially zero-field region ($U_{0i}=U_1$), until the target potential is switched to $U_{0f}>U_1$. In the second acceleration region (width d_2), the field is constant and in the third region (width L), the ion velocity is constant.

that the target voltage was held to a potential of $U_{0i} = 9.0$ kV before the application of the ion extraction pulse and then switched to $U_{0f} = 9.7$ kV. The first grid potential is permanently held at $U_1 = 9.0$ kV and the second grid is grounded. As high voltage switch a HTS 300 (Behlke Electronic GmbH) is used.

The extraction delay, i.e. the time interval between the laser pulse and the actual instant that the extraction field is switched on, was controlled by retarding the laser and switch triggers independently. This delay was measured for each laser shot. Therefore, each spectrum represents one-shot acquisition, avoiding the problems arising from the laser/switch system jitter. The delay was varied in the 0–200 ns range. The dead time for the DE electronics was determined to be 250 ns, which includes about 150 ns for the switch to raise the voltage. This time was measured by using a Tektronix P6015 high voltage probe. It is important to note that this delay extraction set-up allows measurements that probe the plasma expansion since its very beginning (approximately zero delay).

The ion dynamics is simulated numerically for the spectrometer configuration used in the measurements and for a set of initial plume parameters. The TOF peak data is fitted by introducing in the spectrometer ion optics equations the plasma parameters at the end of the second stage, in particular T_{fast}, v_{drift} and the center of plasma when the extraction field was applied. The last two parameters were determined from the model presented in Section 2.

4. Results

Fig. 2 presents the measured Cs^+ TOF spectra for the different delayed fields applied and corresponding to $I_0 = 1.5 \times 10^9$ W cm^{-2}. The evolution of the TOF peak shape as function of the delay time shows an enhancement of the peak tail. The same result was observed for the different laser intensity measurements.

Fig. 3b–d show model predictions for the temporal evolution of the surface and plasma temperatures (T_s and T_p), as well as of the flux of the sublimated particles during the laser-target interaction. Calculations were performed considering a Gaussian-like laser pulse $I_s(t) = I_0 \exp[-(t - t_{max})^2/t_0^2]$, as shown in Fig. 3a. Numerical values are $t_{max} = 10$ ns, $t_0 = 2.2$ ns, $I_{01} = 2.7$, $I_{02} = 2.6$, $I_{03} = 1.9$ and $I_{04} = 1.5$ GW cm^{-2}. The evolution of the T_s as function of time (Fig. 3b) shows a very rapid rise of T_s, leading to temperatures far above the boiling point ($T_s \gg T_b$). Note that the temporal evolution of the sublimated particles flux follows roughly the laser intensity one, as shown in Fig. 3c.

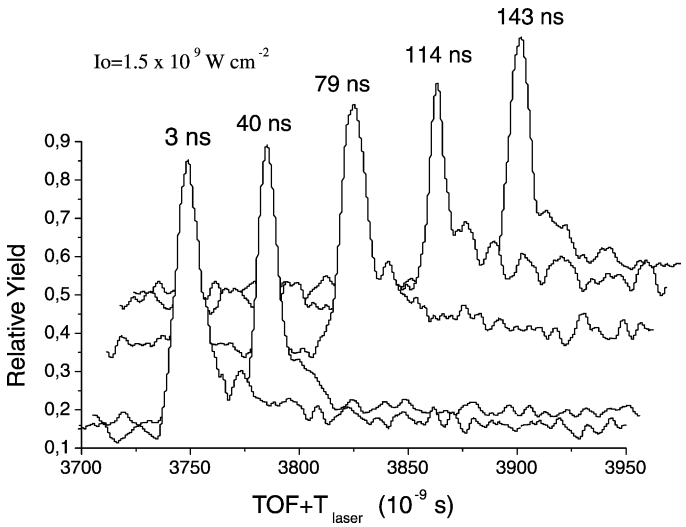

Fig. 2. Cs^+ ion TOF spectra as function of the extraction field delay for $I_{04} = 1.5$ GW cm^{-2}. T_{laser} is the time interval between the master trigger signal and the laser shot.

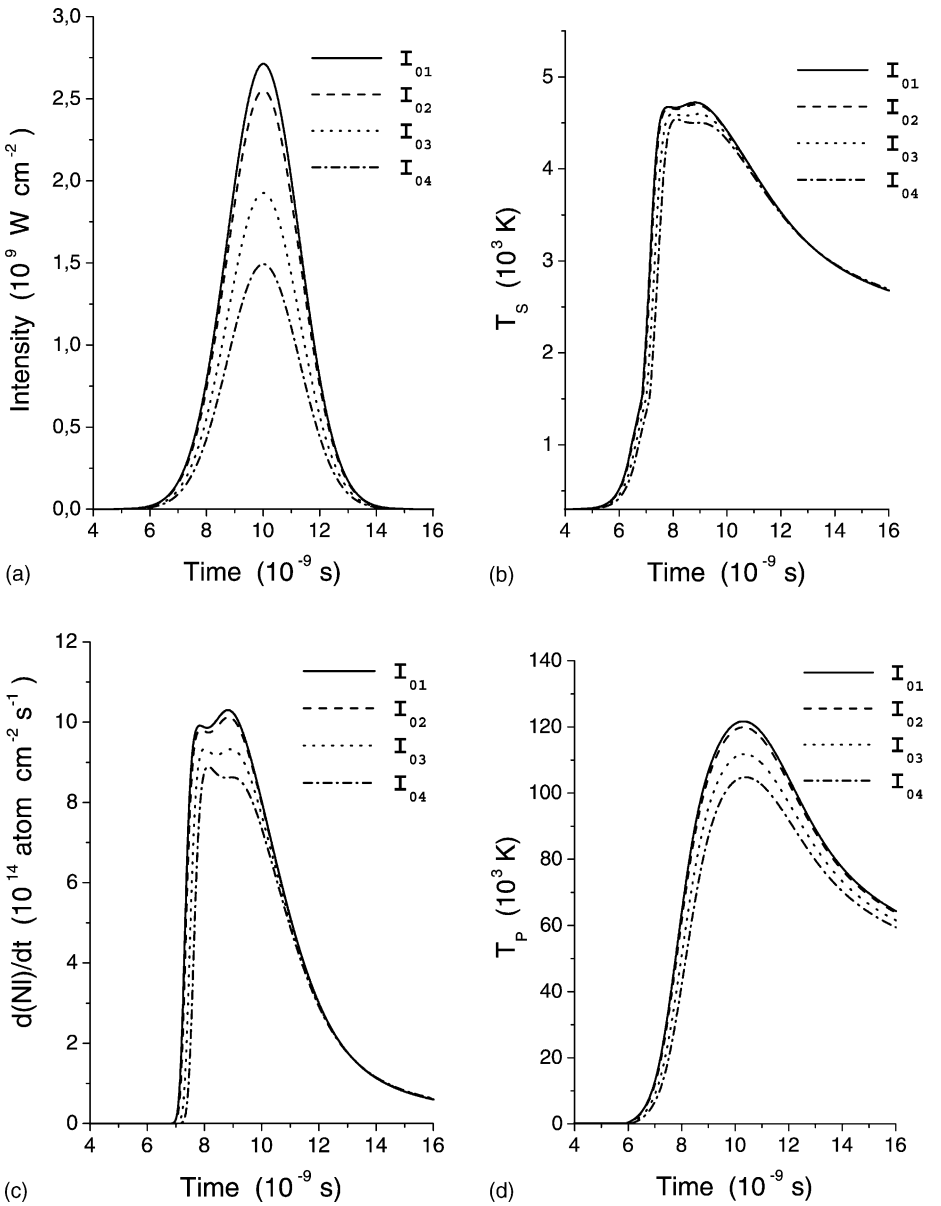

Fig. 3. Model predictions. The temporal evolution of: (a) laser pulse intensities (I_{01} to I_{04}); (b) target surface temperature (T_s); (c) sublimated particles flux (dNl/dt); and (d) plasma temperature (T_p).

At the end of the laser pulse, more than 90% of the plasma is already formed. The plasma temperature (Fig. 3d) reaches values about 20 times higher than the solid temperature and starts to decrease by radiative emission as soon as the laser pulse ends.

In spite of the fact that the laser intensity varies by a factor of 2, the solid temperature evolution practically does not change. At the end of the laser pulse, this intensity variation implies a plasma temperature of only 10%; similarly, the sputtered mass varies of about 30%. This auto-regulation is due to the facts: (i) vapor pressure controls sublimation rate, (ii) there is plasma self-emission and (iii) plasma reflectivity depends on the laser intensity.

The obtained drift velocity values for the four analyzed laser intensities are: $v_{\text{drift}}\,(I_{01}) = 1390\ \text{m s}^{-1}$, drift $(I_{02}) = 1384\ \text{m s}^{-1}$, $v_{\text{drift}}\,(I_{03}) = 1357\ \text{m s}^{-1}$ and $v_{\text{drift}}\ (I_{04}) = 1330\ \text{m s}^{-1}$. For all measurements, the center of mass of the plasma at the end of the laser pulse is located at approximately 10.6 μm from the target surface. These values were used to fit the TOF peaks, permitting the determination of T_{fast}.

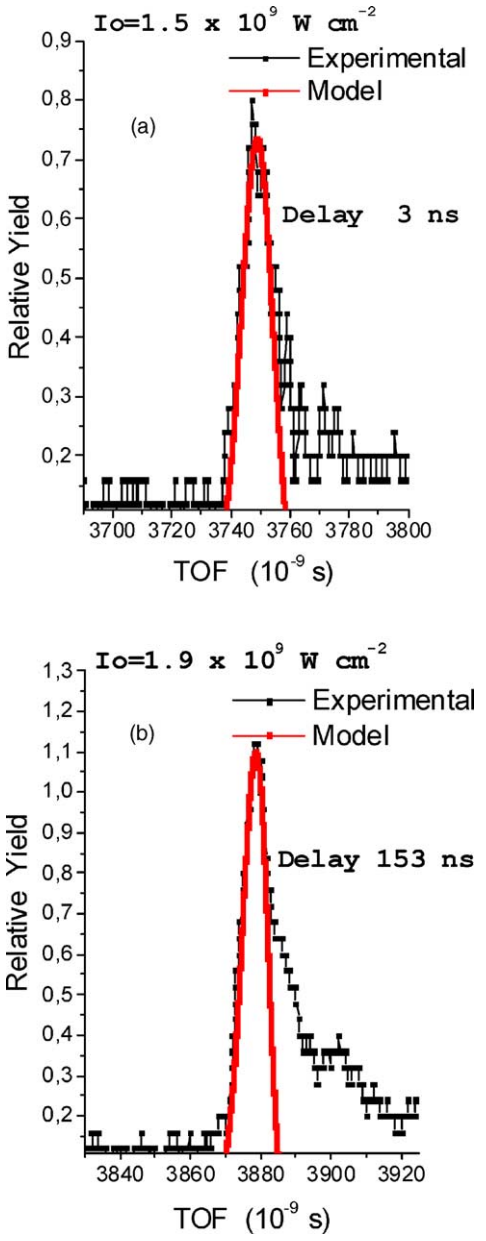

Fig. 4. Illustration of the simulated-measured TOF peak agreement when using: (a) laser intensity of $I_{04} = 1.5\ \text{GW cm}^{-2}$ and 3 ns extraction delay; (b) laser intensity of $I_{03} = 1.9\ \text{GW cm}^{-2}$ and 153 ns extraction delay. From the fast component fitting, the temperature of the plasma in expansion is determined.

In Fig. 4, the comparison of simulation with experimental peak shape is presented for two extreme delays. Generally, measurement-model agreement is good for short extraction delays (Fig. 4a), case in which the slow component is not accentuated. The fast component is well described for short and long delays (Fig. 4b). The observed peak tail behavior of the TOF may be caused by the enhancement of the number of collisions in the plasma during and after the laser pulse. The earlier the ions are removed from the plume, the smaller is the collision effects in the plasma.

Fig. 5 shows the T_{fast} dependence on the extraction delay for the mentioned laser intensities. Again, the results reveal that laser intensity variations do not affect dramatically the plasma temperature evolution.

Finally, it should be mentioned that peaks corresponding to $(\text{CsI})_n\text{Cs}^+$ clusters, with $n = 1$–3, were observed. It has been claimed that in laser induced desorption, the very fast temperature increase $(10^{10}\ \text{K s}^{-1})$ favors emission of aggregates [23].

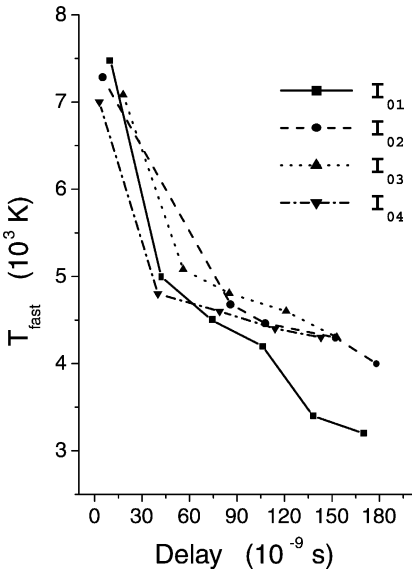

Fig. 5. Plasma temperature (T_{fast}) dependence on delayed extraction time, according to the procedure illustrated in Fig. 4.

An alternative process may be the explosive emission of pre-formed large aggregates.

5. Conclusions

A delay extraction system was used to analyze Cs^+ ion TOF data obtained from UV laser ablation. The set-up allows probing the plasma expansion since the beginning of the expansion. Calculations based on a thermal uni-dimensional model were performed and compared with data. A good agreement was found for the fast component of the TOF peak. The measured ion velocity distribution has approximately a shifted-Gaussian shape; one parameter (v_{drift}), is calculated from this model describing the plasma ionization and expansion, the other parameter (T_{fast}), is determined from the data fitting. It is proposed that T_{fast} represents the plasma temperature in its expansion, from 7000 to 3000 K during the first 200 ns evolution.

Some obvious improvements are necessary in the model, in particular a three-dimensional description and an adiabatic expansion treatment. Then, the angular distribution of the emitted particles can be analyzed and a natural relationship between T_{fast} and v_{drift} could appear. The inclusion of the adiabatic expansion process in the model should reduce enormously the plasma temperature, T_p ($\approx 10^5$ K in the current calculation), approaching it from T_{fast}.

A significant emission of clusters was observed. As this is not predicted by standard evaporation models, other ablation mechanisms should be investigated.

Acknowledgements

The authors want to acknowledge the Centro Latinoamericano de Física, FAPERJ and CNPq for the partial support of this work.

References

[1] D.B. Chrisey, G.K. Hubler (Eds.), Pulsed Laser Deposition of Thin Films, Wiley, New York, 1994.
[2] J.G. Lunney, Appl. Surf. Sci. 86 (1995) 79.
[3] S. Fähler, H.U. Krebs, Appl. Surf. Sci. 96–98 (1996) 61.
[4] G.M. Weyl, in: L.J. Radziemski, D.A. Cremers (Eds.), Laser-Induced Plasmas and Applications, Marcel Dekker, New York, 1989 (Chapter 1).
[5] D.I. Rosen, J. Mitteldorf, G. Kothandaraman, A.N. Pirri, E.R. Pugh, J. Appl. Phys. 53 (1982) 3190.
[6] C.R. Phipps, R.W. Dreyfus, Laser ionization mass analysis, in: A. Vertes, R. Gijbels, F. Adams (Eds.), Chemical Analysis Series, vol. 124, Wiley, 1993 (Chapter 4).
[7] F. Piuz, Nucl. Instrum. Meth. A 371 (1996) 96–115.
[8] J. Almeida, et al., Nucl. Instrum. Meth. A 367 (1995) 332–336.
[9] A. Breskin, Nucl. Instrum. Meth. A 371 (1996) 116–136.
[10] J.G. Lunney, R. Jordan, Appl. Surf. Sci. 127–129 (1998) 941–946.
[11] C.R. Phipps, J. Appl. Phys. 64 (1998) 1083.
[12] X. Mao, R.E. Russo, Appl. Phys. A A64 (1997) 1.
[13] A. Valentini, E. Nappi, M.A. Nitti, Nucl. Instrum. Meth. A 482 (2002) 238–243.
[14] J.F. Ready, Effects of High-Power Laser Radiation, Academic Press, New York, 1971.
[15] H.S. Carslaw, J.C. Jaeger, Conduction of Heat in Solids, Oxford.
[16] D.R. Lide (Ed.), CRC Handbook of Chemistry and Physics, CRC Press, Boca Raton, 1995–1996.
[17] R.E. Kidder, in: P. Caldirola, H. Knoepfel (Eds.), Proceedings of the International School of Physics, Academic Press, New York, 1971, Course 48, pp. 278–305.
[18] Ya.B. Zeldovich, Yu.P. Raizer, Physics of Shock Waves and High-Temperature Hydrodynamics Phenomena, vol. 1, Academic Press, New York, 1966.
[19] R.W.P. McWhirter, in: R.H. Huddlestone, S.L. Leonard (Eds.), Plasma Diagnostic Techniques, Academic, New York, 1965 (Chapter 5).
[20] G.J. Van Wylen, R.E. Sonntag, Fundamentals of Classical Thermodynamics, Wiley, New York, 1985 (Chapter 10).
[21] M.W. Zemansky, Heat and Thermodynamics, McGraw-Hill, New York, 1968 (Chapter 12).
[22] V.M. Collado, Ph.D. Dissertation, Catholic University of Rio de Janeiro, 2001.
[23] L. Hanley, O. Kornienko, E.T. Ada, E. Fuoco, J.L. Trevor, J. Mass Spectrom. 34 (1999) 708.